**Aberystwyth University**

*Accelerating fishes increase propulsive efficiency by modulating vortex ring geometry*

Akanyeti, Otar; Putney, Joy; Yanagitsuru, Yuzo R.; Lauder, George V.; Stewart, William J.; Liao, James C.

# ACCELERATING FISHES INCREASE PROPULSIVE EFFICIENCY BY MODULATING VORTEX RING GEOMETRY.

O. Akanyeti[1,2], Joy Putney[1,3], Y.R. Yanagitsuru[1], G.V. Lauder[4], W.J. Stewart[1,5], J.C. Liao[1]

[1] The Whitney Laboratory for Marine Bioscience, Department of Biology, University of Florida, St. Augustine, FL 32080, USA.

[2] The Department of Computer Science, Aberystwyth University, Ceredigion, SY23 3FL, Wales.

[3] The School of Biological Sciences, Georgia Institute of Technology, Atlanta, GA 30332, USA.

[4] The Department of Organismic and Evolutionary Biology, Harvard University, Cambridge, MA 02138, USA.

[5] The Department of Science, Eastern Florida State College, Melbourne, FL 32935, USA.

Author for correspondence: J.C.L. (jliao@whitney.ufl.edu), O.A. (ota1@aber.ac.uk)

**Abstract**

Swimming animals need to generate propulsive force to overcome drag, regardless of whether they swim steadily or accelerate forward. While locomotion strategies for steady swimming are well characterized, far less is known about acceleration. Animals exhibit many different ways to swim steadily, but we show here that this behavioral diversity collapses into a single swimming pattern during acceleration regardless of the body size, morphology, and ecology of the animal. We draw on the fields of biomechanics, fluid dynamics and robotics to demonstrate that there is a fundamental difference between steady swimming and forward acceleration. We provide empirical evidence that the tail of accelerating fishes can increase propulsive efficiency by enhancing thrust through the alteration of vortex ring geometry. Our study provides new insight into how propulsion can be altered without increasing vortex ring size, and represents a fundamental departure from our current understanding of the hydrodynamic mechanisms of acceleration. Our findings reveal a unifying hydrodynamic principle that is likely conserved in all aquatic, undulatory vertebrates.

45 **Significance Statement**

46 The ability to move is one of the key evolutionary events that led to the complexity of vertebrate

47 life. The most speciose group of vertebrates, fishes, displays an enormous variation of movement

48 patterns during steady swimming. We discovered that this behavioral diversity collapses into one

49 movement pattern when fishes are challenged to increase their swimming speed, regardless of

50 their body size, shape and ecology. Using flow visualization and biomimetic models, we

51 provide the first mechanistic understanding of how this conserved movement pattern allows

52 fishes to accelerate quickly.

53 \body

54

**Introduction**

Over the course of evolutionary time, patterns of animal locomotion have diversified to take advantage of the physical environment through the interplay of morphology, physiology and neural control. Yet, two fundamental principles of locomotion in most animals remain the same: 1) Force is generated by transferring momentum to the environment through repetitive motions such as body undulations and oscillating appendages (legs, fins, or wings), and 2) the locomotor speed is modulated by controlling the amplitude and frequency of these periodic motions (1, 2). Previous studies have demonstrated that the degrees of freedom in amplitude and frequency control are not limitless, but rather constrained by the physical laws imposed by the environment. For example, flying animals must maintain a high wing-beat frequency to generate enough lift, controlling speed primarily by altering the wing's angle of attack(3). In contrast, the morphology and locomotion strategies of aquatic animals have adapted to moving through a viscous environment where gravitational forces are negligible. Among these strategies, the ancestral state of aquatic locomotion is axial undulation, where muscle contractions bend the body into a mechanical wave that passes from head to tail (4). The interaction of angled body surfaces with the surrounding fluid propels the animal forward, and the movements of the entire body contribute to the overall swimming performance (5-10).

Over the past several decades, a number of studies have investigated the kinematics (11-14), muscle activity (15-18) and hydrodynamics (19-21) of tail movements, in particular how tail beat amplitude and frequency are controlled during steady swimming. Most undulatory vertebrates such as fishes, alligators, dolphins and manatees control speed by primarily modulating tail beat frequency while maintaining a relatively low tail beat amplitude (22-25). At high steady swimming speeds, tail beat amplitude reaches a plateau at around 0.2 body length

78  (*L*). Computational studies (26-29) and experiments with hydrofoils (30, 31) suggest that

79  swimming animals operate in this range to maintain high swimming efficiency.

80      How do these mechanisms apply when a steadily-swimming animal accelerates forward,

81  which is often used to catch prey, avoid predators or save energy during migrations (32, 33)?

82  One hypothesis is that speed is gained only by further increasing the tail beat frequency (34-37).

83  Alternatively, an animal can bend its body maximally to accelerate large amounts of fluid, as

84  seen in Mauthner initiated C-starts (38-41).  Yet emerging studies suggest that forward

85  acceleration exhibits distinct kinematics (42-46) that defy both hypotheses, indicating that

86  acceleration may have its own optimization strategy. Although forward acceleration has been a

87  topic of interest for decades in the field of aquatic locomotion (39, 43), a comprehensive

88  understanding of its prevalence and underlying mechanisms has remained elusive. Here, we

89  identify a new undulatory locomotion strategy for forward acceleration by integrating

90  complementary approaches: biological experiments with live fishes and physical experiments

91  with bio-mimetic fish models.

92

93

94

95

## Results and Discussion

<u>Acceleration kinematics across fish phylogeny</u>

We discovered that in fishes tail beat amplitude is consistently higher during acceleration than during steady swimming (Fig. 1). This pattern is conserved across 51 species examined, with representatives from a wide range of phylogenetic positions from chondrichthyes (e.g. bonnethead shark, *Sphyrna tiburo*) to tetraodontiformes (e.g. stripped burrfish, *Chilomycterus schoepfi*). These species exhibit vastly different body shapes, ecological habitats and swimming modes (Table S1). Some species use median or pectoral fins during steady swimming (e.g. clown knifefish, *Chitala ornata* and sergeant major, *Abudefduf saxatilis*), but always revert to body undulation when they accelerate forward from steady swimming.

When we plot tail beat amplitude during acceleration against steady swimming for all species, we found that the relationship is linear (Fig. S1a). This suggests that the relative increase in tail beat amplitude during acceleration is constant at 34±4%. However, there is substantial variation in the absolute amplitude values that depends on body length and shape. For example, when body length is held constant, elongate fishes such as Florida gar (*Lepisosteus platyrhincus*) and Northern barracuda (*Sphyraena borealis*) accelerate with lower tail beat amplitudes (0.19±0.01 *L*) compared to more fusiform fishes such as tarpon and red drum (0.24±0.01 *L*). We also found that during acceleration tail beat amplitude decreases with body length (Fig. S1b). To better understand if there is a common propulsive strategy across fish diversity, we next performed a more detailed midline analysis of the entire body during steady swimming and forward acceleration for 9 species. Despite extreme differences in body shape and swimming mode, we found that all fishes share similar midline acceleration kinematics. These acceleration bouts are usually brief, typically less than five tail beats. All points along the body show higher

119  amplitudes compared to steady swimming, but not as high as seen during C-starts (39, 40) (Fig.

120  S2-4). Further analyses on the travelling body wave and tail movement suggest efficient force

121  production during acceleration (Table S2). The average values across 10 species for slip ratio,

122  Strouhal number (St) and maximum angle of attack ($\alpha_{max}$) are 0.80±0.02, 0.41±0.01, and

123  22.71±0.65˚, respectively. Slip ratios approaching 1 reveal high swimming efficiency, while

124  experiments with thrust-producing, harmonically oscillating foils show that propulsive efficiency

125  is maximized when St falls within the range of 0.2 and 0.5 and $\alpha_{max}$ is between 15˚ and 25˚ (30).

126       In addition to the species studied here, similar acceleration kinematics was previously

127  observed in American eels (44). These elevated amplitudes are most notable around the head and

128  tail. The onset of acceleration (which can be easily recognized because of strong head yaw and a

129  faster tail beat) provides a reference point to interpret the phase relationship between head and

130  tail. By doing so, we found that the motion of the head always precedes the motion of the tail,

131  indicating that the body wave is initiated by strong head movements in all species, though the

132  timing between head and tail movements is not constant. To more closely investigate the

133  kinematics and hydrodynamics of acceleration, we chose a generalized teleost fish, the rainbow

134  trout (*Oncoryhnchus mykiss*). The swimming kinematics of this species has been studied in great

135  detail for steady swimming and other behaviors but not for acceleration (5, 13, 47-54). Like other

136  species tested in this study, the body amplitudes of trout are higher during acceleration than

137  during steady swimming (Fig. S5a), and head movements precede the motion of the tail (Fig.

138  S5b).

139       We next examined how swimming speed and acceleration depend on tail beat amplitude,

140  given that a range of amplitudes is evident for each behavior (Fig. S5c). As others have shown

141  previously (44), we found that in general tail beat frequency, not tail beat amplitude, has the

142    most effect during both behaviors (Fig. S5d). Multiple regression analysis revealed that steady

143    swimming speed increases only with tail beat frequency. This trend is similar during

144    acceleration, though tail beat amplitude also has a minor effect (Table S3). Our results suggest

145    that tail beat amplitude does not change during steady swimming or acceleration, but jumps

146    discretely by ~30% when fish transition from one behavior to another. Thus, trout appear to have

147    two undulatory gears based on tail beat amplitude; one for steady swimming and another for

148    acceleration. Our results suggest that this discrete jump in tail beat amplitude during acceleration

149    is correlated with increased head yaw (Fig. S5e), and these movements are tightly phase-locked,

150    with the head preceding the tail (Fig. S5f).

151

152    <u>Hydrodynamic effects of increased tail beat amplitude during acceleration</u>

153         We next investigated how increased tail beat amplitude relates to thrust production and

154    propulsive efficiency by using a combination of quantitative flow visualization experiments on

155    live fish and experiments with actuated, soft-bodied robotic models. Results from particle image

156    velocimetry show that fish can reach a maximum acceleration rate of 20 $L$ s$^{-2}$ from initial

157    swimming speed of 3 $L$ s$^{-1}$. To accomplish this, fish transfer more axial momentum to the fluid

158    by generating stronger vortices compared to steadily swimming fish (Fig. 2a). Similar wake

159    structures were previously observed in zebrafish (55), eel  (44) and carp (45). In addition, fish

160    entrain more fluid around their posterior body to strengthen shed vortices (Fig. 2b). This occurs

161    because the posterior body has a greater curvature, which creates a low pressure region in the

162    concavity (Fig. 2b, t=12.5 ms). The entrained fluid in this low pressure region (blue) follows the

163    traveling body wave until it reaches the trailing edge of the tail (t=50 ms). At the point when the

164    tail reverses direction, the fluid starts to roll off the tail and into the wake (t=56.3 ms).

165 Concurrently, the body concavity causes flow to build up on the opposite side. This fluid (red)

166 starts getting released to the wake as the tail increases its velocity (t = 68.8 ms). When the tail

167 reaches its maximum velocity a vortex is formed (t=81.3 ms), owing to the occurrence of two

168 bodies of fluid moving in opposite directions. Our results indicate that during acceleration body

169 undulations of trout are responsible for increased wake velocity and vorticity. This is not

170 surprising as multiple studies have shown that body-induced flows can enhance vortex shedding

171 in other species (7, 8, 10, 19, 56, 57).

172       When fish swim, they generate vortex rings (58-60). We see this in two dimensions as

173 two counter-rotating vortices (i.e. vortex cores) in the wake after each tail beat (61-63). In recent

174 years, estimating locomotive forces from wake measurements has garnered much interest with

175 hopes of better understanding the resultant motion of the animal (41, 56, 64-66). Several

176 methods have been proposed to estimate locomotive forces (56, 64, 67, 68). The one which we

177 used in this study is based on the classical vortex ring theory (69). We calculated the impulse

178 (i.e. the average force) applied to the fluid during each tail beat by measuring the circulation, jet

179 angle ($\theta$), core diameter ($D_o$) and the spacing between the two vortex cores ($D$). We found that

180 an accelerating trout generates an impulse (along the swimming direction) that is at least 4 times

181 higher than that required for its initial steady swimming speed (Fig. 2c). This higher impulse is

182 due to 172 ±16% increase in vorticity. In addition, the jet angle is oriented ~30±3% more

183 downstream, which devotes a greater proportion of the impulse along the swimming direction.

184       We found that $D$ is reduced by ~25% from 0.33 $L$ to 0.25 $L$ when fish transition from

185 steady swimming to acceleration. At first glance this may be surprising given that the impulse

186 and kinetic energy of a ring is proportional to its size. However, impulse and energy also depend

187 on the geometry of the vortex ring itself. One key parameter of the ring geometry is the ratio

188    between minor and major axis diameters ($d/D$). When $d/D$ approaches one, the ring becomes

189    more axisymmetric, which is favorable because axisymmetric rings possess the maximum

190    amount of energy relative to other shapes that maintain the same total impulse (70, 71). Given

191    that $d$ is always constrained by the span of the tail (7, 58, 59, 62, 72), the axisymmetry of the ring

192    primarily depends on $D$. Our results show that during steady swimming trout generate elliptical

193    rings ($d/D$=0.66). In contrast, we found that during acceleration the geometry of the vortex rings

194    become more axisymmetric ($d/D$=0.88).

195          The impulse of a vortex ring is also proportional to the ratio of its core diameter to its

196    ring diameter ($D_o/D$). In addition to having a more axisymmetric shape, we found that the vortex

197    rings generated by accelerating trout have thicker cores ($D_o/D$=0.37±0.02) than those generated

198    by trout swimming steadily ($D_o/D$=0.25±0.01). It has been shown that for vortex rings generated

199    by a piston pushing a cylinder of fluid through a nozzle there is a limit in generating thicker arms

200    efficiently, because at some point (piston stroke to diameter ratio>3.5) separation occurs and

201    energy dissipated by a trailing edge of fluid (73-75). For finite-core, axisymmetric vortex rings

202    which propagate steadily (76), this piston stroke to diameter ratio corresponds to $D_o/D = 0.42$ in

203    a vortex ring (77, 78). Perhaps not coincidentally, the vortex rings generated by accelerating

204    trout have $D_o/D$ close to 0.42. In order to evaluate whether our fish-generated vortex rings during

205    acceleration can be compared to nozzle-generated rings, we analyzed their velocity and vorticity

206    distributions along a center line connecting the two vortex cores, and confirmed that they closely

207    match the values reported for nozzle-generated rings (73, 79) (Fig. S6a-c). In addition, we

208    investigated the temporal dynamics of vortex rings once they are shed into the wake, and found

209    that they translate downstream with a constant velocity while preserving their $D_o/D$ ratio (Fig.

210  S6d). What this suggests is that the hydrodynamic principles of efficient thrust production in

211  oscillating fish may be similar to those observed during biological jet propulsion (65, 80-82).

212      Overall, our findings indicate that accelerating trout generate more thrust, not by

213  generating larger rings but, by modulating their geometry and orientation. To investigate how

214  common this phenomenon is, we analyzed $d/D$, $D_o/D$ and $\theta$ of four additional species with

215  different swimming modes and body shapes and found similar results (Table S3). In addition,

216  flow imaging on a similar sized American eel ($L$=23 cm) shows that during acceleration

217  anguilliform swimmers also generate vortex rings with comparable $D_o/D$ ratio (~0.4 based on

218  Fig. 1b in (44)). It remains to be seen, however, how $D_o/D$ ratio scales with body size, given that

219  it is significantly higher (0.6-0.7) for smaller fish such as zebrafish (83) and koi carps (45). Note

220  that a 2-dimensional geometric analysis of vortex rings provides an initial, albeit qualitative

221  understanding on how fishes accelerate efficiently. Concatenated, ring-like structures involved in

222  the wakes of fishes can be highly elongated and 3-dimensional, and may not have the same

223  properties (e.g. momentum, energy, and stability) as nozzle-generated rings.

224

225  Relationship between tail kinematics and vortex ring geometry We next propose a set of

226  equations to provide a mechanistic understanding of how the geometry ($d/D$ and $D_o/D$) and angle

227  ($\theta$) of a vortex ring depend on the tail kinematics. Because the oscillating tail generates each core

228  of a vortex ring successively, we used trigonometric relations to define $D = \sqrt{a^2 + b^2}$ and

229  $\theta = \tan^{-1}\left(\frac{a}{b}\right)$, where $a$ and $b$ are the vertical and horizontal spacing between the two cores,

230  respectively. Based on our wake analysis, the vertical spacing depends on the tail beat amplitude

231  (i.e. $a$ = half of the tail beat amplitude), and the horizontal spacing depends on the tail beat

232  frequency and swimming speed (i.e. $b$ = swimming speed multiplied by half tail beat cycle).  To

233 validate our approach, we calculated $D$ and $\theta$ for trout swimming steadily at 3 $L$ s$^{-1}$ and

234 accelerating from the same initial speed. During acceleration we assumed that the swimming

235 speed was 4 $L$ s$^{-1}$ (i.e. the average between initial and final swimming speeds). We compared the

236 predicted $D$ and $\theta$ to those measured experimentally, and found a good match (Fig. 2D, $D$=0.31

237 $L$ and $\theta$=75.07° during steady swimming and $D$=0.22 $L$ and $\theta$=63.43° during acceleration).

238 Once we validated our approach, we used it to further investigate the contribution of increased

239 tail beat amplitude during acceleration. We computationally explored an alternative scenario

240 where the tail beat amplitude was kept constant at the value observed for steady swimming (0.16

241 $L$), and speed was gained by further increasing the tail beat frequency (i.e. hypothetical

242 acceleration). Given that thrust is proportional to the square of tail beat frequency multiplied by

243 the square of tail beat amplitude (84, 85), we increased the tail beat frequency from 10 Hz to

244 12.5 Hz in order to maintain the same effective thrust. We found that this had no effect on the

245 ring angle ($\theta$=63.43°), but generated a suboptimal $D$=0.18 $L$ with $d/D$=1.22 and $D_o/D$=0.56 (we

246 assumed that $d$=0.22 $L$ and $D_o$=0.1 $L$). Therefore, we believe that the increase in tail beat

247 amplitude observed in trout is the key to geometrically generating the most efficient rings.

248

249 <u>The swimming performance of robotic models increases with tail beat amplitude</u>

250      While it is favorable to generate more thrust by producing vortex rings with optimal

251 geometry, this does not reveal the overall swimming efficiency of an accelerating fish because

252 motions that produce them may be costly. It is not unreasonable to imagine that large lateral

253 body amplitudes would incur large drag penalties (44, 45). To resolve this tradeoff, we employed

254 experiments with a biomimetic trout model to systematically explore how different tail beat

255 amplitudes affect steady swimming and acceleration performance (Fig S7). This level of

256    experimental control is impossible to achieve with live fish. We generated undulatory

257    movements in our flexible fish model from a single actuation point located just posterior to the

258    head. Therefore, we were able to control tail beat amplitude by modulating the head yaw.

259         We first measured performance during steady swimming and acceleration at yaw

260    amplitudes very similar to those of live fish (10° and 20°). We found that during steady

261    swimming the model performed better when it is actuated with smaller yaw (Fig. S8a). However,

262    during acceleration this relationship is reversed; swimming performance is consistently higher

263    with larger yaw (Fig. S8b). This suggests that there is no convergence of optimum head yaw

264    between steady swimming and acceleration. While steady swimming seeks to preserve

265    momentum by streamlining motions, during acceleration additional momentum must be

266    generated despite drag costs.

267         To determine if there are yaw values that maximize swimming efficiency during

268    acceleration, we measured efficiency at yaw amplitudes between 0° and 30° at 3° increments.

269    We found that efficiency increases linearly with yaw amplitudes up to 20°, beyond which values

270    plateau (Fig. 3). When we map head yaw from live fish onto our model performance curve, we

271    found that increasing head yaw from steady swimming values to acceleration values can create

272    an increase in efficiency up to 100%. It is perhaps no accident that the yaw amplitudes chosen by

273    accelerating fish fall within the range that gives greatly increased propulsive efficiency compared

274    to steady swimming. We hypothesize that this is due to generating hydrodynamically more

275    efficient vortex rings, based on our flow measurements in the wake of live fishes. However,

276    increasing head yaw to accelerate with more optimal vortex rings does not mean that producing

277    these rings costs less than the rings produced during steady swimming (Figure S9 shows a 50%

278    increase in mechanical power input for increased head yaw).

13

279    The ability to move is one of the key evolutionary events that led to the diversity and

280    complexity of vertebrate life. Given that movement through fluids is energetically costly, fishes

281    have found many ways to minimize drag during normal, steady swimming, such as keeping the

282    body straight and using median or paired fin locomotion (86-88). While steady swimming is

283    optimized for endurance by minimizing the energetic investment, acceleration favors

284    maximizing force production to escape quickly from predators or capture elusive prey. Here, we

285    show that the enormous behavioral diversity observed during steady swimming collapses into a

286    single locomotion strategy when fishes transition to forward acceleration. We believe that this

287    strategy is likely conserved across all undulatory swimmers and not just fishes because it is

288    hydrodynamically the optimal solution to maximize propulsive efficiency.

**Methods**

289

290

291 All research protocols were approved by the Institutional Animal Care and Use Committee at the

292 University of Florida. All data analyses were performed in Matlab (Mathworks) and all values

293 are shown as mean ± standard error of the mean, unless stated otherwise.

294

295 <u>Diversity of swimming kinematics across species</u> Our data set included 51 species of salt and

296 freshwater fish (105 individuals, from 20 taxonomic orders), which were either obtained from

297 commercial dealers or wild caught using cast net or hook-and-line. The details about these

298 species are given in Table S1, and the research protocols are described in Text S1.

299

300

301 <u>Swimming hydrodynamics of rainbow trout</u> We used digital particle image velocimetry to

302 quantify the flow fields around and behind steady swimming and accelerating trout. We

303 estimated wake forces as described in (66) (see Text S2 for more details on the experimental

304 procedures and data analysis).

305

306 <u>Experiments with the physical fish model</u> We performed the experiments in the flow tank at

307 Harvard University which is customized to house a computer-controlled external actuator. We

308 used this system in the past to evaluate the swimming performance in a number of swimming

309 mechanical models (5, 89-91). Here, we systematically moved the physical model with different

310 tail kinematics and measured the total sum of forces acting on the whole body. For these

311    measurements, we calculated the propulsive force produced by the model and the corresponding

312    power output of the actuator as described in (92) (see Text S3 for more details).

**References**

1. Alexander RM (2003) *Principles of Animal Locomotion* (Princeton University Press).
2. Biewener (2003) *Animal Locomotion* (Oxford University Press).
3. Nudds RL, Taylor GK, & Thomas ALR (2004) Tuning of Strouhal number for high propulsive efficiency accurately predicts how wingbeat frequency and stroke amplitude relate and scale with size and flight speed in birds. *Proceedings Royal Society London B* 271:2071-2076.
4. Gray J (1953) The locomotion of fishes. *Essays in Marine Biology*, eds Marshall SM & Orr AP (Oliver and Boyd, Edinburgh), pp 1-16.
5. Akanyeti O*, et al.* (2016) Fish optimize sensing and respiration during undulatory swimming. *Nature Communications* 7.
6. Gemmell BJ, Collin SP, Costello JH, & Dabiri JO (2015) Suction-based on propulsion as a basis for efficient animal swimming. *Nature communications* 6(8790).
7. Kern S & Koumoutsakos P (2006) Simulations of optimized anguilliform swimming. *The Journal of Experimental Biology* 209:4841-4857.
8. Müller UK, Smit J, Stamhuis EJ, & Videler JJ (2001) How the body contributes to the wake in undulatory fish swimming: flow fields of a swimming eel (*Anguilla anguilla*). *The Journal of Experimental Biology* 204:2751-2762.
9. Nauen JC & Lauder GV (2001) Three-dimensional analysis of finlet kinematics in the chub mackerel (*Scomber japonicus*). *The Biological Bulletin* 200(1):9-19.
10. Borazjani I & Sotiropolous F (2009) Numerical investigation of the hydrodynamics of anguilliform swimming in the transitional and inertial flow regimes. *Journal of Experimental Biology* 212:576-592.
11. Bainbridge R (1958) The speed of swimming of fish as related to size and to the frequency and amplitude of the tail beat. *The Journal of Experimental Biology* 35:109-133.
12. Videler JJ & Hess F (1984) Fast continuous swimming of two pelagic predators, saithe (*Pollachius virens*) and mackerel (*Scomber scombrus*): a kinematic analysis. *The Journal of Experimental Biology* 109:209-228.
13. Webb PW, Kostecki PT, & Stevens ED (1984) The effect of size and swimming speed on the locomotor kinematics of rainbow trout. *The Journal of Experimental Biology* 109:77-95.
14. Jayne BC & Lauder GV (1995) Speed Effects on Midline Kinematics During Steady Undulatory Swimming of Largemouth Bass, *Micropterus salmoides*. *The Journal of Experimental Biology* 198(2):585-602.
15. Rome LC, Swank D, & Corda D (1993) How fish power swimming. *Science* 261:340-343.
16. Jayne BC & Lauder GV (1996) New data on axial locomotion in fishes: how speed affects diversity of kinematics and motor patterns. *American Zoologist* 36(6):642-655.
17. Altringham J & Ellerby DJ (1999) Fish swimming: patterns in muscle function. *The Journal of Experimental Biology* 202(Pt 23):3397-3403.
18. Coughlin DJ (2002) Aerobic muscle function during steady swimming in fish. *Fish and Fisheries* 3:63-78.
19. Videler JJ, Müller UK, & Stamhuis EJ (1999) Aquatic vertebrate locomotion: Wakes from body waves. *The Journal of Experimental Biology* 202(23):3423-3430.
20. Drucker EG & Lauder GV (2002) Experimental Hydrodynamics of Fish Locomotion: Functional Insights from Wake Visualization. *Integrative and Comparative Biology* 42(2):243-257.

367 21. Lauder GV & Tytell ED (2005) Hydrodynamics of Undulatory Propulsion. *Fish Physiology*,
368 (Academic Press), Vol Volume 23, pp 425-468.
369 22. Bainbridge R (1963) Caudal fin and body movements in the propulsion of some fish. *The
370 Journal of Experimental Biology* 40:23-56.
371 23. Fish FE (1984) Kinematics of Undulatory Swimming in the American Alligator. *American
372 Society of Ichthyologists and Herpetologists* 4:839-843.
373 24. Fish FE (1998) Comparative kinematics and hydrodynamics of odontocete cetaceans:
374 morphological and ecological correlates with swimming performance. *Journal of Experimental
375 Biology* 201:2867-2877.
376 25. Kojeszewski T & Fish FE (2007) Swimming kinematics of the Florida manatee (*Trichechus
377 manatus latirostris*): hydrodynamic analysis of an undulatory mammalian swimmer. *Journal of
378 Experimental Biology* 210:2411-2418.
379 26. Eloy C (2013) On the best design for undulatory swimming. *Journal of Fluid Mechanics*
380 717:48-89.
381 27. Schultz WW & Webb PW (2002) Power Requirements of Swimming: Do New Methods
382 Resolve Old Questions? *Integrative and Comparative Biology* 42:1018-1025.
383 28. van Rees WM, Gazzola M, & Koumoutsakos P (2015) Optimal morphokinematics for
384 undulatory swimmers at intermediate Reynolds numbers. *Journal of Fluid Mechanics* 775:178-
385 188.
386 29. Tytell ED, Hsu C-Y, Williams TL, Cohen AH, & Fauci LJ (2010) Interactions between
387 internal forces, body stiffness, and fluid environment in a neuromechanical model of lamprey
388 swimming. *National Academy of Sciences* 107(46):19832–19837.
389 30. Anderson JM, Streitlien K, Barrett DS, & Triantafyllou MS (1998) Oscillating foils of high
390 propulsive efficiency. *Journal of Fluid Mechanics* 360:41-72.
391 31. Taylor GK, Nudds RL, & Thomas AL (2003) Flying and swimming animals cruise at a
392 Strouhal number tuned for high power efficiency. *Nature* 425(6959):707-711.
393 32. Weihs D & Webb PW (1983) Optimization of Locomotion. *Fish Biomechanics*, eds Webb
394 PW & Weihs D (Praeger Publishers, New York).
395 33. Gleiss AC*, et al.* (2011) Convergent evolution in locomotory patterns of flying and swimming
396 animals. *Nature Communications* 2.
397 34. Rome LC*, et al.* (1988) Why animals have different muscle fibre types. *Nature* 335:824 - 827.
398 35. Johnson TP, Syme DA, Jayne BC, Lauder GV, & Bennett AF (1994) Modeling red muscle
399 power output during steady and unsteady swimming in largemouth bass. *American Journal of
400 Physiology- Regulatory, Integrative and Comparative Physiology* 267(2 pt 2):R481-R488.
401 36. Weihs D (1974) Energetic Advantages of Burst Swimming of Fish. *Journal of Theoretical
402 Biology* 48:215-229.
403 37. Videler JJ & Weihs D (1982) Energetic advantages of burst-and-coast swimming of fish at
404 high speeds. *Journal of Experimental Biology* 97:169-178.
405 38. Eaton RC, Bombardieri RA, & Meyer DL (1977) The Mauthner-initiated startle response in
406 teleost fish. *Journal of Experimental Biology* 66(1):65-81.
407 39. Domenici P & Blake RW (1997) The Kinematics and Perforemcance of Fish Fast-Start
408 Swimming. *The Journal of Experimental Biology* 200(pt 8):1165-1178.
409 40. Wakeling JM (2006) Fast-start mechanics. *Fish Biomechanics*, eds Shadwick RE & Lauder
410 GV (Academic Press, San Diego), pp 333-368.
411 41. Tytell ED & Lauder GV (2008) Hydrodynamics of the escape response in bluegill sunfish,
412 *Lepomis macrochirus*. *Journal of Experimental Biology* 211:3359-3369.

413    42.Fierstine HL & Walters V (1968) Studies in locomotion and anatomy of scombroid fishes.
414    *Memoirs of the Southern California Academy of Science* 6:1-31.
415    43.        Videler JJ (1993) *Fish Swimming* (Chapman and Hall, New York).
416    44.Tytell ED (2004) Kinematics and hydrodynamics of linear acceleration in eels, *Anguilla*
417    *rostrata. Philosophical Transactions Royal Society London B* 271:2535-2540.
418    45.Wu G, Yang Y, & Zeng L (2007) Kinematics, hydrodynamics and energetic advantages of
419    burst-and-coast swimming of koi carps (*Cyprinus carpio koi*). *Journal of Experimental Biology*
420    210:2181-2191.
421    46.van Leeuwen JL, Lankheet MJM, Akster HJ, & Osse JWM (1990) Function of red axial
422    muscles of carp (*Cyprinus carpio* L.): recruitment and normalized power output during
423    swimming in different modes. *Journal of Zoology London* 220(123-145).
424    47.Drucker EG & Lauder GV (2003) Function of pectoral fins in rainbow trout: behavioral
425    repertoire and hydrodynamic forces. *Journal of Experimental Biology* 206(Pt 5):813-826.
426    48.Drucker EG & Lauder GV (2005) Locomotor function of the dorsal fin in rainbow trout:
427    kinematic patterns and hydrodynamic forces. *The Journal of Experimental Biology* 208(Pt
428    23):4479-4494.
429    49.Coughlin DJ (2000) Power production during steady swimming in largemouth bass and
430    rainbow trout. *The Journal of Experimental Biology* 203:617-629.
431    50.Ellerby DJ & Altringham JD (2001) Spatial variation in fast muscle function of the rainbow
432    trout Oncorhynchus mykiss during fast-starts and sprinting. *The Journal of Experimental Biology*
433    204(Pt 13):2239-2250.
434    51.Liao JC, Beal DN, Lauder GV, & Triantafyllou MS (2003) The Kármán gait: novel body
435    kinematics of rainbow trout swimming in a vortex street. *The Journal of Experimental Biology*
436    206(6):1059-1073.
437    52.Akanyeti O & Liao JC (2013) Effect of flow speed and body size on Kármán gait kinematics
438    in rainbow trout. *The Journal of Experimental Biology* 216:3442-3449.
439    53.Stewart WJ, Tian F, Akanyeti O, Walker CJ, & Liao JC (2016) Refuging rainbow trout
440    selectively exploit flows behind tandem cylinders. *Journal of Experimental Biology*
441    219(14):2182-2191.
442    54.Akanyeti O & Liao JC (2013) A kinematic model of Kármán gaiting in rainbow trout. *The*
443    *Journal of Experimental Biology* 216(24):4666-4677.
444    55.Müller UK, Stamhuis EJ, & Videler JJ (2000) Hydrodynamics of unsteady fish swimming
445    and the effects of body size: Comparing the flow fields of fish larvae and adults. *The Journal of*
446    *Experimental Biology* 203(2):193-206.
447    56.Tytell ED & Lauder GV (2004) The hydrodynamics of eel swimming: I. Wake structure
448    *Journal of Experimental Biology* 207:1825-1841.
449    57.Gemmell BJ*, et al.* (2016) How the bending kinematics of swimming lampreys build negative
450    pressure fields for suction thrust. *Journal of Experimental Biology* 219:3884-3895.
451    58.Flammang BE, Lauder GV, Troolin DR, & Strand TE (2011) Volumetric imaging of fish
452    locomotion. *Biology Letters* 7(5):695-698.
453    59.Mendelson L & Techet AH (2015) Quantitative wake analysis of a freely swimming fish
454    using 3D synthetic aperture PIV. *Experiments in Fluids* 56(135):1-19.
455    60.Tytell ED, Standen EM, & Lauder GV (2008) Escaping Flatland: three dimensional
456    kinematics and hydrodynamics of median fins in fishes. *Journal of Experimental Biology*
457    211(2):187-195.

458    61.Blickhan R, Krick C, Zehren D, Nachtigall W, & Breithaupt T (1992) Generation of a vortex
459    chain in the wake of a Subundulatory swimmer. *Naturwissenschaften* 79(5):220-221.
460    62.Nauen JC & Lauder GV (2002) Hydrodynamics of caudal fin locomotion by chub mackerel,
461    *Scomber japonicus* (Scombridae). *The Journal of Experimental Biology* 205(12):1709-1724.
462    63.Müller UK, Van den Heuvel BLE, Stamhuis EJ, & Videler JJ (1997) Fish foot prints:
463    morphology and energetics of the wake behind a continuously swimming mullet (*Chelon*
464    *labrosus Risso*). *The Journal of Experimental Biology* 200(22):2893-2906.
465    64.Drucker EG & Lauder GV (1999) Locomotor forces on a swimming fish: three-dimensional
466    vortex wake dynamics quantified using digital particle image velocimetry. *Journal of*
467    *Experimental Biology* 202(Pt 18):2393-2412.
468    65.Bartol IK, Krueger PS, Stewart WJ, & Thompson JT (2009) Hydrpdynamics of pulsed jetting
469    in juvenile and adult brief squid Lolliguncula brevis: evidence of multiple jet 'modes' and their
470    implication of propulsive efficiency. *Journal of Experimental Biology* 212:1889-1903.
471    66.Epps BP & Techet AH (2007) Impulse generated during unsteady maneuvering of swimming
472    fish. *Experiments in Fluids* 43:691-700.
473    67.Noca F, Shiels D, & Jeon D (1999) A comparison of methods for evaluating time-dependent
474    fluid dynamic forces on bodies, using only velocity fields and their derivatives. *Journal of Fluids*
475    *and Structures* 13:551-578.
476    68.Dabiri JO (2005) On the estimation of swimming and flying forces from wake measurements.
477    *Journal of Experimental Biology* 208:3519-3532.
478    69.Batchelor GK (2000) *An Introduction to Fluid Dynamics* (Cambridge University Press).
479    70.      Kelvin L (1880) Vortex statistics. *Philosophical Magazine* 10:97-109.
480    71.Dabiri JO (2009) Optimal vortex formation as a unifying principle in biological propulsion.
481    *Annual Review of Fluid Mechanics* 41:17-33.
482    72.Borazjani I & Daghooghi M (2013) The fish tail motion forms an attached leading edge
483    vortex. *The Royal Society Proceedings B* 280(1756):20122071.
484    73.Gharib M, Rambod E, & Shariff K (1998) A universal time scale for vortex ring formation.
485    *Journal of Fluid Mechanics* 360:121-140.
486    74.Krueger PS & Gharib M (2005) Thrust augmentation and vortex ring evolution in a fully
487    pulsed jet. *The Journal of American Institute of Aeronautics and Astronautics* 43(4):792-801.
488    75.Mohseni K & Gharib M (1998) A model for universal time scale of vortex ring formation.
489    *Physics of Fluids* 10:2436-2438.
490    76.Norbury J (1973) Family of steady vortex rings. *Journal of Fluid Mechanics* 57:417-431.
491    77.Linden PF & Turner JS (2004) 'Optimal' vortex rings and aquatic propulsion mechanisms.
492    *Proceedings of The Royal Society B* 271(1539):647-653.
493    78.Linden PF & Turner JS (2001) The formation of `optimal' vortex rings, and the efficiency of
494    propulsion devices. *Journal of Fluid Mechanics* 427:61-72.
495    79.Weigand A & Gharib M (1997) On the evolution of laminar vortex rings. *Experiments in*
496    *Fluids* 22:447-457.
497    80.Dabiri JO, Collin SP, Katija K, & Costello JH (2010) A wake-base correlate of swimming
498    performance and foraging behavior in seven co-occurring jellyfish species. *Journal of*
499    *Experimental Biology* 213:1217-1225.
500    81.Gharib M, Rambod E, Kheradvar A, Sahn DJ, & Dabiri JO (2006) Optimal vortex formation
501    as an index of cardiac health. *Proceedings of the National Academy of Sciences of the United*
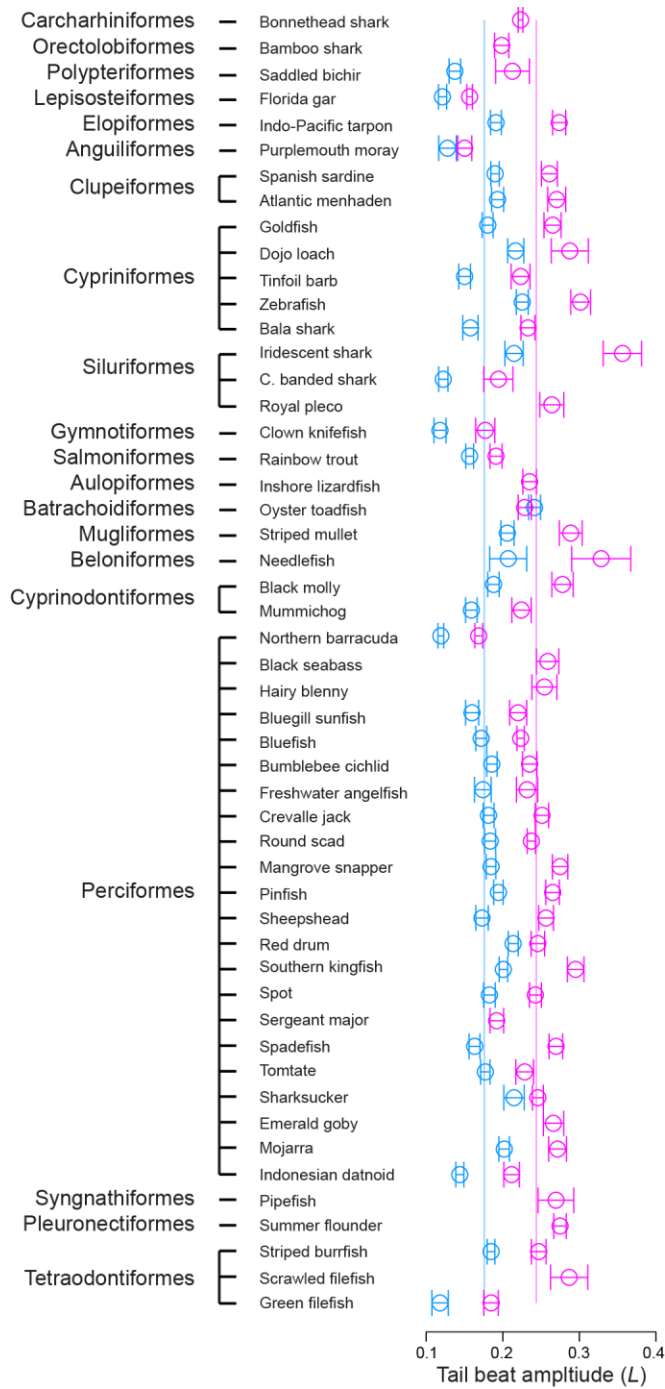502    *States of America* 103:6305-6308.

503    82.Dabiri JO, Collin SP, & Costello JH (2006) Fast-swimming hydromedusae exploit velar
504    kinematics to form an optimal vortex wake. *Journal of Experimental Biology* 209:2025-2033.
505    83.Müller UK & van Leeuwen JL (2004) Swimming of larval zebrafish: ontogeny of body waves
506    and implications for locomotory development. *The Journal of Experimental Biology* 207(Pt
507    5):853-868.
508    84.Wu TY (1977) Introduction to scaling of aquatic animal locomotion. *Scale Effects of Animal
509    Locomotion*, ed Pedley TJ (Academic Press, New York, NY), pp 203-232.
510    85.Lighthill J (1971) Large-amplitude elongated body theory of fish locomotion. *Proceedings of
511    the Royal Society B: Biological Sciences* 179(1055):125-138.
512    86.Lighthill J (1993) Estimates of Pressure Differences across the Head of a Swimming Clupeid
513    Fish. *Philosophical Transactions of the Royal Society B: Biological Sciences* 341(1296):12.
514    87.Webb PW (1992) Is the high cost of body/caudal fin undulatory swimming due to increased
515    friction drag or inertial recoil? *The Journal of Experimental Biology* 162:157-166.
516    88.Fish FE (1998) Imaginative solutions by marine organisms for drag reduction. *Proceedings of
517    the International Symposium on Seawater Drag Reduction*:443-450.
518    89.Lauder GV, Flammang BE, & Alben S (2012) Passive robotic models of propulsion by the
519    bodies and caudal fins of fish. *Integrative and Comparative Biology* 52:576-587.
520    90.Shelton RM, Thornycroft JMP, & Lauder VG (2014) Undulatory locomotion of flexible foils
521    as biomimetic models for understanding fish propulsion. *Journal of Experimental Biology*
522    217:2110-2120.
523    91.Lauder GV & Tangorra JL (2015) Fish locomotion: biology and robotics of body and fin-
524    based movements. *Robot Fish - Bioinspired Fishlike Underwater Robots*, eds Du R, Li Z,
525    Youcef-Toumi K, & Valdivia Y Alvarado P (Springer-Verlag, Berlin), pp 25-49.
526    92.Read DA, Hover FS, & Triantafyllou MS (2003) Forces on oscillating foils for propulsion
527    and maneuvering. *Journal of Fluids and Structures* 17:163-183.
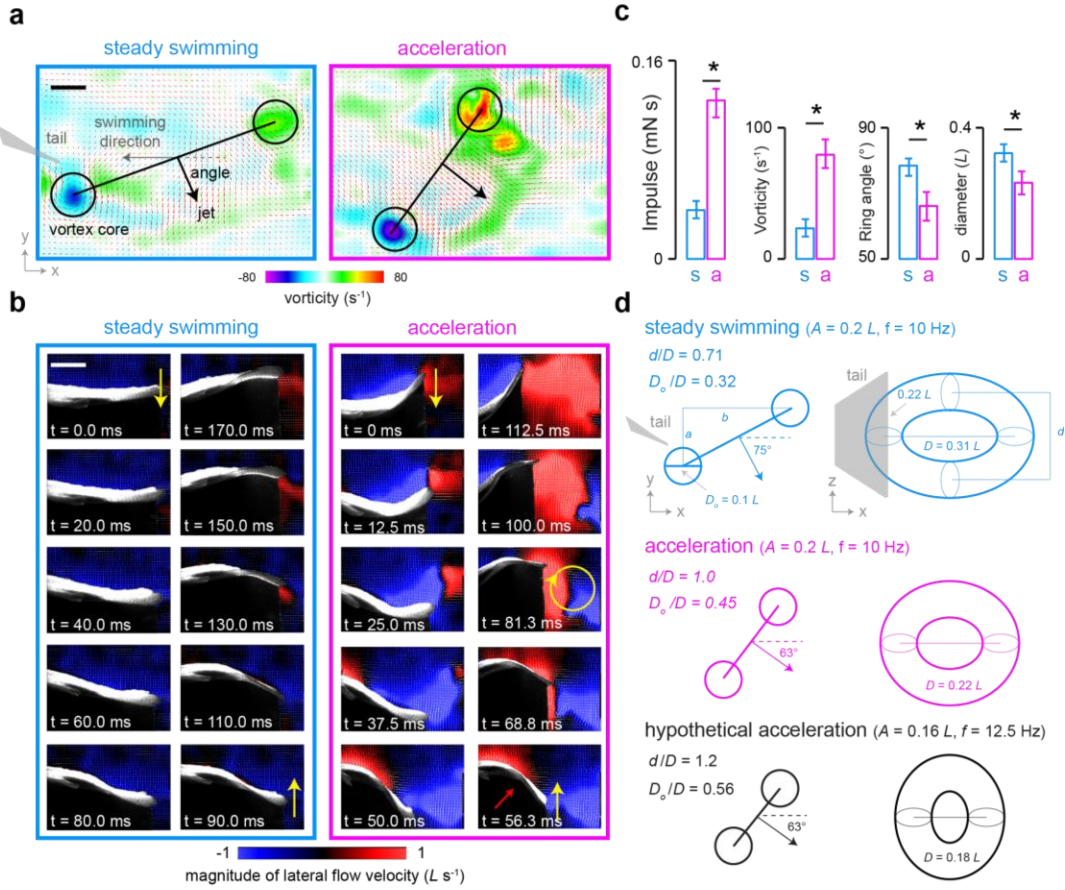528
529
530

531

533 Figure 1



534
535

536     Figure 2.

537

538

**a**

steady swimming    acceleration

swimming
direction

tail

angle

jet

vortex core

y
x

−80    80
vorticity (s⁻¹)

**b**

steady swimming    acceleration

t = 0.0 ms     t = 170.0 ms
t = 20.0 ms    t = 150.0 ms
t = 40.0 ms    t = 130.0 ms
t = 60.0 ms    t = 110.0 ms
t = 80.0 ms    t = 90.0 ms

t = 0 ms       t = 112.5 ms
t = 12.5 ms    t = 100.0 ms
t = 25.0 ms    t = 81.3 ms
t = 37.5 ms    t = 68.8 ms
t = 50.0 ms    t = 56.3 ms

−1    1
magnitude of lateral flow velocity ($L$ s⁻¹)

**c**

Impulse (mN s)     Vorticity (s⁻¹)     Ring angle (°)     diameter ($L$)

*                  *                    *                 *

s  a               s  a                 s  a              s  a

**d**

steady swimming ($A$ = 0.2 $L$, f = 10 Hz)
$d/D$ = 0.71
$D_o/D$ = 0.32

tail

$b$
$a$
75°
$D_o$ = 0.1 $L$

y
x

tail

0.22 $L$

$D$ = 0.31 $L$

$d$

z
x

acceleration ($A$ = 0.2 $L$, f = 10 Hz)
$d/D$ = 1.0
$D_o/D$ = 0.45

63°

$D$ = 0.22 $L$

hypothetical acceleration ($A$ = 0.16 $L$, f = 12.5 Hz)
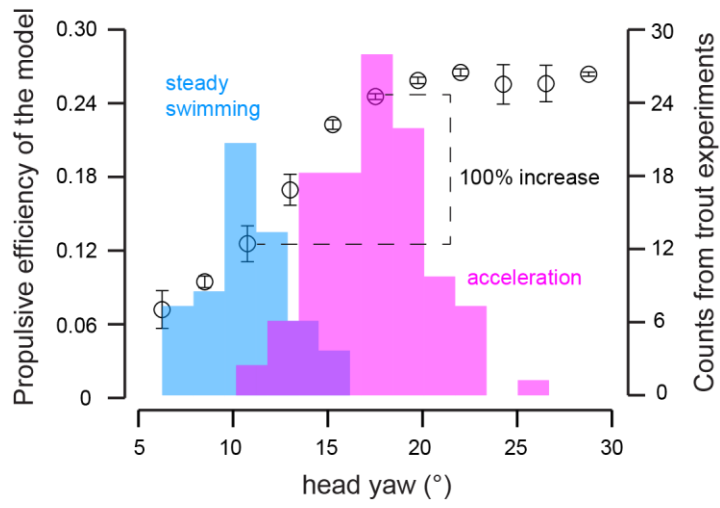$d/D$ = 1.2
$D_o/D$ = 0.56

63°

$D$ = 0.18 $L$

539
540

25

541    Figure 3.



542

**Figure Legends**

544

545   Figure 1. Fishes have higher tail beat amplitude during acceleration. (a) This phenomenon was

546   confirmed across a wide range of fishes from 20 taxonomic orders with different body shapes,

547   swimming modes and ecologies. Blue and magenta lines indicate the mean tail beat amplitudes

548   for steady swimming (0.181 ± 0.004 *L*) and acceleration (0.244 ± 0.006 *L*), respectively. Mean

549   tail beat amplitudes for steady swimming and acceleration are statistically different (unpaired T-

550   test, *P*<0.001). During steady swimming, it was not possible to measure the tail beat amplitude

551   of few species (black seabass, sergeant major, pipefish, summer flounder and filefish), as they

552   use primarily median or pectoral fins for propulsion. Error bars are ± one standard error of the

553   mean.

554    Figure 2. Hydrodynamics of steady swimming versus acceleration. (a) Representative flow fields

555    behind a rainbow trout ($L$=32 cm) swimming steadily at 3 $L$ s$^{-1}$ (left) and accelerating (right)

556    from the same initial speed. The heat map denotes vorticity where negative (magenta) and

557    positive (red) values indicate clockwise and counter-clockwise rotation, respectively. The length

558    of the scale bar is 2 cm. (b) Body movements of the same fish during steady swimming (left

559    column) and acceleration (right column) over one representative tail beat cycle. Yellow arrows

560    indicate the direction of tail movement. The blue and red denote the magnitude of left and right

561    flow fields, respectively, in the fish frame of reference. In each video frame, the body of the trout

562    is visible from the dorsal fin to the tail, which represents the 30% of the total length. The length

563    of the scale bar is 4.5 cm. (c) Mean impulse, vorticity, angle and diameter of an average vortex

564    ring for steady swimming and acceleration (10 tail beats from each fish, n=2 fish). * denotes

565    significant at $P$<0.01, unpaired T-test. Error bars are ± one standard error. (d) Hypothesized

566    vortex ring geometry and orientation behind fish swimming steadily (blue) and accelerating

567    (magenta). Hypothetical acceleration with lower tail beat amplitude is also shown for

568    comparison (black).

569

570   Figure 3. Fishes adopt acceleration kinematics tuned for high propulsive efficiency. Propulsive

571   efficiency of the physical model as a function of head yaw at flow speed 1.2 $L\,\text{s}^{-1}$ (left axis, black

572   points; error bars are ± one standard error); propulsive efficiency increases with increasing head

573   yaw. A histogram of head yaw (right axis) is shown for live trout during steady swimming (blue)

574   and acceleration (magenta). Note that the overlapped region between the distributions steady

575   swimming and acceleration appears darker. The average head yaw for steady swimming and

576   acceleration is 12.469± 0.370° and 17.805±0.352°, respectively (unpaired T-test, $P<0.01$).

577